Two-variable nullcline analysis of ionic general equilibrium predicts calcium homeostasis in ventricular myocytes

David Conesa[1☯], Blas Echebarria[1] , Angelina Peñaranda[1], Inmaculada R. Cantalapiedra[1], Yohannes Shiferaw[2] , Enrique Alvarez-Lacalle[1,☯,*]

1 Departament de Física. Universitat Politècnica de Catalunya-BarcelonaTech, Barcelona. Spain
2 Physics Department. California State University Northridge. Los Angeles. United States.

☯These authors contributed equally to this work.
* enric.alvarez@upc.edu

Abstract

Ventricular contraction is roughly proportional to the amount of calcium released from the Sarcoplasmic Reticulum (SR) during systole. While it is rather straightforward to measure calcium levels and contractibility under different physiological condition, the complexity of calcium handling during systole and diastole has made the prediction of its release at steady state impossible. Here we approach the problem analyzing the evolution of intracellular and extracellular calcium fluxes during a single beat which is away from homeostatic balance. Using an in-silico subcellular model of rabbit ventricular myocyte, we show that the high dimensional nonlinear problem of finding the steady state can be reduced to a two-variable general equilibrium condition where pre-systolic calcium level in the cytosol and in the SR must fulfill simultaneously two different equalities. This renders calcium homeostasis as a problem that can be studied in terms of its equilibrium structure, leading to precise predictions of steady state from single-beat measurements. We show how changes in ionic channels modify the general equilibrium as shocks would do in general equilibrium macroeconomic models. This allows us to predict when an enhanced entrance of calcium in the cell reduces its contractibility and explain why SERCA gene therapy, a change in calcium handling to treat heart failure, might fail to improve contraction even when it successfully increases SERCA expression.

Author summary

Cardiomyocytes, upon voltage excitation, release calcium, which leads to cell contraction. However, under some pathological conditions, calcium handling is impaired. Recently, SERCA gene therapy, whose aim is to improve Ca2+ sequestration by the Sarcoplasmic Reticulum (SR), has failed to improve the prognosis of patients with Heart Failure. This, together with recent counterintuitive results in calcium handling, has highlighted the need for a framework to understand calcium homeostasis across species and pathologies. We show here that the proper framework is a general equilibrium approach of two independent variables. The development of this framework allows us to find a possible mechanism for the failure of SERCA gene therapy even when it manages to increase Ca SERCA expression.

Introduction

Complex systems often present robust regulation that makes them resilient to changes in environmental conditions. Despite the presence of a large number of nonlinearly interacting elements, averaged quantities in these sytems often attain predictable, and sometimes constant, values. Examples range from ecosystems and climate regulation to long-run macroeconomics [1, 2]. Our bodies present a good example of such behavior. The maintenance of homeostatic equilibrium in temperature, pH, osmolality or ionic concentration is crucial to sustaining life, and complex feedback mechanisms have been developed to achieve such goal.

Another important example is the regulation of heart function. Fundamental for survival is the ability of the heart to contract and expel more blood by increasing the heart rhythm [3]. In most animal species the amount of blood pumped at each beat increases with beat rate, which stems from a positive correlation between contractile force and beating frequency [4–6]. However, the variability of the force-frequency relation is quite large across species, being quite flat for some, like mouse and rat [7, 8]. As the contraction machinery in the sarcomeres is activated by an increase in intracellular calcium, this variability is determined by differences in calcium handling [9–11]. During the action potential of the heart, calcium enters into the cell via L-type calcium channels (LCC) triggering the release of calcium stored in the sarcoplasmic reticulum (SR). This process, called calcium-induced calcium-release (CICR), seems universal across species, although quantitatively can be very different. Not just the release of calcium is species dependent, its reuptake into the SR by the SR Ca^2 ATPase (SERCA) and the extrusion of calcium from the cell by the sodium-calcium exchanger (NCX) also differs. Translation of results obtained in animal models targeting different regulatory pathways into human patients is thus not trivial.

To reach homeostatic equilibrium, the amount of calcium entering the cell must be compensated by the quantity extruded [12, 13]. Equally, the amount of calcium released from the SR during the transient must be the same reuptaken by SERCA [12, 14]. Global equilibrium is thus determined by a balance of global fluxes, that encompass the complex internal machinery of calcium release, composed of thousands of interacting release units. A good understanding of calcium homeostasis is necessary to understand the effect of changes in calcium handling regulatory mechanisms. In particular, dysregulations in calcium homeostasis have important implications for arrhythmias since calcium overload of the SR often facilitates the initiation of calcium alternans, calcium waves, and arrhythmogenic EADs [13, 15–17].

Altered expression and/or functionality of proteins involved in calcium dysregulation, has often been treated with therapeutic strategies as gene therapy [18]. In particular, SERCA gene therapy has been successfully applied to preclinical treatment of heart failure (HF) in animals, showing an increase in SERCA2a expression and improved cardiac function [19, 20]. In humans, despite early promising results [21, 22], more recent studies with wider samples of patients have found no statistical effects of the treatment [23]. These unsuccessful results have been related to reduced viral gene transfer in humans and the effect of neutralizing antibodies present in patients. However, one can not disregard the possibility that SERCA therapy may fail even when SERCA function is improved since its failure or success also depends on how the underlying pathology affects the general equilibrium properties of calcium homeostasis. Highlighting also the relevance of undestanding calcum homeostasis in order to predict calcium levels when some channel properties are changed, recent reviews [12, 24] have shown clear anti-intuitive calcium behavior. For example, an increase in entrance of calcium via LCC is not always followed by an increase in total calcium levels at the steady state.

To clarify why the calcium behavior seems often anti-intuitive and show its very

complex nature we can use that precise example. Consider that, in a cell under constant pacing, the conductance of the L-type calcium channels is suddenly increased. Naively, one would expect this to lead to an increase in SR calcium load, as more calcium enters the cell, and gets accumulated into the SR. This is indeed often the case, as our simulations show for a detailed model of calcium handling in rabbit myocytes (see Fig. 1 and details of the model in the next section). It is not too difficult, however, to modify the model with changes in the levels of buffers and SERCA, and obtain counterintuitive results. In this modified model, as the strength of LCC increases, the SR Ca concentration decreases as seen in Fig. 2. In this case, a larger entrance of calcium into the cell produces a larger release from the SR, that then is taken more efficiently out of the cell by NCX, resulting in a net efflux of calcium from the cell. This counterintuive result (described experimentally in [25]) is not at all unique. It seem clear that understanding and predicting calcium homeostatic levels is key to understand the contractibility behavior of cardiac ventricles.

Fig 1. Structure of the computational ventricular rabbit cardiomyocyte model Panel (1): Scheme of the three-dimensional model where the cardiomyocyte is divided into thousands of 3d stacked Calcium Release Units (highlighted one in red). Panel (2): Depiction of the basic structure of the CaRU's showing the L-type Calcium Channels (LCC) in front of the Ryanodine Receptor (RyR), the SERCA pump and the Na-Ca Exchanger. The different states of the LCC and the RyR2 are also depicted. Panel (3): Typical cytosolic (orange) and SR (blue) free calcium transients in the rabbit ventricular model (described in Methods) at a voltage-clamped pacing rate of 2 Hz

Fig 2. Example of anti-intuitive calcium homeostatic regulations Panel (1): Evolution of the SR free calcium concentration when, at a time marked by a black vertical line, the conductivity of the LCC is increased (left) or decreased (right). An increase in intake via the LCC leads to a cardiomyocyte with higher calcium average concentrations in the SR. Panel (2): Response of the cardiomyocyte to an increase in LCC conductivity, as in the first panel, when its buffering and SERCA uptake is different. Now, the increased intake via LCC is homeostatically regulated in a completely different way. The higher level of calcium intake leads to an even larger extrusion for the SR leading to a lower calcium load.

Materials and methods

Rabbit computational model structure

We consider the cell to be a 3-dimensional array composed of $25 \times 25 \times 50$ Calcium Release Units (CaRUs) of volume $0.5 \times 0.5 \times 2\mu m^3$ following the basic structure described in [26] (see first panel in Fig. 1) where the cell is divided into volumes associated with RyR cluster. However, we introduce key modifications to ensure mass conservation, a property that we have found lacking in all the models published in the literature. As in previous models, each CaRU is divided into 5 compartments or subvolumes as shown in the second panel of Fig. 1: cytosol (i), subsarcolemma (s), network sarcoplasmic reticulum (sr), junctional sarcoplasmic reticulum (jsr) and dyadic junction (d), which is the space between a group of LCC (L-type Calcium Channels), in the cellular membrane, and a cluster of Ryanodine Receptors (RyR), in the membrane of the sarcoplasmic reticulum. The basic structure of the CaRU is not a cube with dz being the distance between Z-planes which we take to be roughly 2 μm [27,28] while the

distance in X-Y is the average distance between large clusters of RyR (40) or the aggregation scales of smaller ones that we take to be 500 nm [29, 30].

This model considers the diffusion of calcium ions between compartments of the same CaRU, as well as diffusion between neighboring CaRUs; moreover, there are other currents related to the dynamics of calcium buffers, thus differentiating between free and attached-to-buffers calcium ions in the different compartments. Finally, there are currents due to channels, exchangers or pumps. L-type calcium channels introduce calcium, j_{LCC}, in the dyadic space. Flux across RyR also goes into the dyadic from the junctional SR, j_{RyR}. SERCA pumps calcium j_{SrCa} from the cytosol to the SR and the Na^+/Ca^{2+} exchanger is considered to be in the membrane and t-tubules as LCC but not close to it. We, therefore, consider that the exchanger flux, j_{NCX}, is sensible to the calcium gradient between extracellular calcium and calcium concentrations in the subsarcolemma. The dynamics are deterministic except for the RyRs and LCCs which are defined by internal markovian states and whose transitions are considered to be stochastic. A detailed model of the states is described in the following sections.

The set of differential equations for Ca^{2+} concentration in the different compartments on each CaRU (where we have omitted the $i, j, k-$th superscripts indexing the position of the CaRUs for simplicity) reads as follows, where we take no-flux boundary conditions:

$$\frac{dc_d}{dt} = j_{RyR} - j_{LCC} - j_{ds} \tag{1}$$

$$\frac{dc_s}{dt} = j_{NCX} - j_{si} + \frac{v_d}{v_s} j_{ds} + D_s \nabla^2 c_s \tag{2}$$

$$\frac{dc_i}{dt} = -j_{SrCa} + \frac{v_s}{v_i} j_{si} - j_{buff_i} + D_i \nabla^2 c_i \tag{3}$$

$$\frac{dc_{jsr_{TOT}}}{dt} = j_{tr} - \frac{v_d}{v_{jsr}} j_{RyR} \tag{4}$$

$$\frac{dc_{sr}}{dt} = -j_{tr} + \frac{v_i}{v_{sr}} j_{SrCa} + D_{sr} \nabla^2 c_{sr} \tag{5}$$

where j_{ds}, j_{si}, j_{tr} represent internal diffusion currents and v_d, v_s, v_i, v_{jsr} and v_{sr} represent local volumes for dyadic space, subsarcolemma, cytosol, junctional SR and SR respectively. We take the cytosolic volume to be half of the available space ($0.25\ \mu m^3$) given the presence of mitochondria which we neglect in this model. D_s, D_i and D_{sr} are the inter-CaRU diffusion constants for subsarcolemma, cytosol, and SR respectively. In the case of subsarcolemmal diffusion, we consider that these volumes do not exist across z-planes so $(D_s)_z = 0$. Regarding D_i and D_{sr}, they are different from each other, slower in the SR, but the same in all directions. Notice, however, that given that the characteristic length is different across the z-plane direction, the characteristic time scales of diffusion in the Z direction is different than in the X-Y direction.

The model spatial structure considers 3 different diffusive currents within a CaRU, which depend only on the difference of Ca^{2+} concentration among the affected compartments with a given characteristic time of diffusion. These are: Diffusion between dyadic junction and subsarcolemma, $j_{ds} = \frac{c_d - c_s}{\tau_d}$. Diffusion between subsarcolemma and cytosol, $j_{si} = \frac{c_s - c_i}{\tau_s}$. Diffusion between network and junctional sarcoplasmic reticulum, $j_{tr} = \frac{c_{sr} - c_{jsr}}{\tau_{tr}}$.

The above equations have to be complemented with calcium buffers and the external clamped potential which fixes an external pacing. In this model, the pacing of the model is set by a periodic clamped action potential with a constant pacing period T and an action potential duration APD. We define the membrane potential as

$$V(t) = \begin{cases} (V_{max} - V_{rest})\sqrt{1 - (\frac{\widetilde{t}}{APD})^2} + V_{rest}, & \text{if } \widetilde{t} < \text{APD} \\ V_{rest}, & \text{if } \widetilde{t} > \text{APD} \end{cases} \quad (6)$$

where $\widetilde{t} = t - nT$, with n = 0, 1, 2...Voltage affects the calcium intake via LCC j_{LCC} since increases in voltage open the channel while extrusion of calcium via j_{NCX} is favored when voltage is down. The details of this volage-dependent will be described in susequent sections.

The resulting intake of calcium each time voltage raises due to the opening of LCC raises the probability of RyR2 to open, releasing calcium from the SR during the depolarization of voltage (systole), the well-known Calcium-Induced Calcium-release (CICR) mechanism, which then binds to TnC triggering contraction. Once the voltage is repolarized calcium released from the SR is uptaken by SERCA back to the SR while NCX is able to extrude the calcium which entered via LCC and contraction ceases. This process happens probabilistically at each CaRU, resulting in an averaged behavior as the one depicted in the third panel of Fig.1. Average free calcium concentration values in the cytosol raise and drop during one beat (calcium transient) while in the SR a transient drop in the concentration of free calcium is followed by its recovery.

Regarding buffering we must stress that our model presents a very important difference with previous models. We do not take fast-buffering approximations anywhere since this leads to a loss in the conservation of mass in the dynamical equations and it does not particularly slow down the code. Buffers are located by construction in the cytosol and in the junctional SR. The above equations have to be complemented with the equivalent equation for the calcium going into the buffers dynamically as we will see in the next subsection. We have, surprisingly, not found any discussion regarding the lack of conservation of mass in codes using fast-buffering approximation described in the literature. In our analysis, it is critical to have an algorithm that strictly conserves mass to all orders. This also leads us to consider jSR to be the volume around the RyR where calsequestrin is present and to compute the evolution of $c_{jsr_{TOT}}$, which includes both free calcium in jSR, c_{jsr} and calcium attached to calsequestrin in that compartment. The reason is that calsequestrin is the only buffer that is fast enough to slow down the performance of the code if the attachment of calcium to the buffer would be computed dynamically. Once the total amount of calcium is computed in the jSR, this calcium is split between the free and buffered parts using the fast-buffering approximation solving a quadratic equation. All the other buffers have their own dynamical equation where the calcium taken out from its free level goes to the calcium attached to the buffer as indicated.

Mass conservation in calcium models. Buffering.

Buffering currents in the model are present only in the cytosol and depend on binding (k_{on}) and unbinding (k_{off}) rates of calcium in the buffers b, and also on the concentration of buffers, B_b, and concentration of Ca^{2+} bound to them, c_b. These currents are computed by adding the contribution of all the buffers in the compartment :

$$j_{buff_i} = \sum_b j_b = \sum_b k_{on_b} c_i (B_b - c_b) - k_{off_b} c_b \quad (7)$$

while Ca^{2+} concentration attached to buffer b, c_b follows the equation

$$\frac{dc_b}{dt} = k_{on_b} c_i (B_b - c_b) - k_{off_b} c_b = j_b \quad (8)$$

where j_b is the contribution of buffer b to the buffering current j_{buff_i}. Notice that we do not use the rapid buffering approximation in any of the buffers of the cytosol.

The reason is that fast buffering approximation leads to a loss of mass in any type of propagation algorithm we have considered. The lack of conservation of mass in models with fast buffering approximation seems to be not known in the literature but it is clear that any Euler algorithm does not conserve mass to all orders. Using fluxes we can enforce with the Euler's algorithm that the exact amount of calcium that leaves one compartment place is placed in another compartment, in a buffer or goes outside of the cell. All in all, the changes in total calcium in the cell come exactly from the differences between the calcium that enters the cell and the amount that leaves it.

The initial condition of calcium concentration attached to this buffer is taken as if it was in equilibrium with free calcium concentration:

$$c_b(t=0) = \frac{k_{on_b} B_b c_i(t=0)}{k_{off_b} + k_{on_b} c_i(t=0)} \tag{9}$$

but it is let to evolve dynamically.

We consider five buffers in the cytosol. The buffering which is proper of the SERCA pump, Calmodulin, buffers in the internal membrane structures (SLH), Tropomyosin C (TnC) and the dye buffering which we take to be similar in properties to Fluo-4. We do not take into account any buffer in the dyadic volume since they are considered to be non-existent there and we neglect the effect of buffers in the subsarcolemma for simplification.

Dynamics of buffering in the junctional sarcoplasmic reticulum in our model is restricted to calsequestrin (CSQ) which is considered to have very fast dynamics and in equilibrium. Thus, we need to obtain the free Ca^{2+} concentration in jsr without using the standard buffering approximation which does not conserve mass. At each time step the total amount of calcium in the jsr $c_{jsr_{TOT}}$ is obtained and then we consider fast equilibrium approximation. Therefore

$$c_{jsr_{TOT}} = c_{jsr} + \frac{c_{jsr} B_{CSQ}}{c_{jsr} + K_{CSQ}} \tag{10}$$

where B_{CSQ} is the concentration of calsequestrin in the jsr and K_{CSQ} its dissociation constant. The free calcium concentration c_{jsr} can be obtained solving the quadratic equations:

$$c_{jsr} = \frac{1}{2}(c_{jsr_{TOT}} - (K_{CSQ} + B_{CSQ}) + \sqrt{(K_{CSQ} + B_{CSQ} - c_{jsr_{TOT}})^2 + 4K_{CSQ} c_{jsr_{TOT}}}) \tag{11}$$

Time scales and affinities are mostly taken from Bers reference [31] and SR and SLH buffer adjusted slightly so that typical experimental values of the maximum in the rabbit calcium transient are reproduced [3, 32].

Currents of rabbit model

Calcium extrusion (Na^+/Ca^{2+} Exchanger) and intake (LCC)

The current associated to Na^+/Ca^{2+} exchanger depends on intracellular and extracellular Na^+ concentrations ($[Na]_i$ and $[Na]_o$ respectively), which are set as constant in voltage-clamped model, as well as on extracellular Ca^{2+} concentration ($[Ca]_o$), also constant, and subsarcolemmal calcium concentration c_s. Its expression reads

$$j_{NCX} = \frac{g_{NaCa}}{1 + (K_{da}/c_s)^3} \frac{e^{\eta z}[Na]_i^3[Ca]_o - e^{(\eta-1)z}[Na]_o^3 c_s}{S(c_s)(1 + k_{sat} e^{(\eta-1)z}} \tag{12}$$

where

$$S(c_s) = [Na]_o^3 c_s + K_{mNao}^3 c_s[1 + (c_s/K_{mCai}] + K_{mCao}[Na]_i^3 + \\ + [Na]_i^3[Ca]_o + K_{mCai}[Na]_o^3[1 + ([Na]_i/K_{mNai})^3] \quad (13)$$

and z=$\frac{VF}{RTemp}$, with V being the membrane voltage, F the Faraday constant, R the ideal gas constant and $Temp$ the temperature.

The current produced by the LCC channels taking calcium from the extracellular medium towards the intracellular depends on the voltage, the extracellular Ca^{2+} concentration and the calcium in the dyadic volume, the one close to both the RyR cluster and the LCC channels. The current is proportional to the number of LCC channels in open state (O_{LCC}) . We use the expression given in [26] for the properties of LCC in rabbit. In each CaRU we consider a group of 5 LCC channels, where each one of them can be in one of 5 possible states as shown in the second panel of Fig.1: O for the open state, C1 and C2 for closed states, and I1 and I2 for inactivated states. Here we track the state of each one of the channels using the length rule to establish a transition between states with the uniformly distributed random number generator RANMAR. The expression of this current reads:

$$j_{LCC} = g_{CaL} O_{LCC} 4 z_m \frac{e^{2z} c_d - [Ca]_o}{e^{2z} - 1} \quad (14)$$

where z is still $z = \frac{VF}{RTemp}$ and $z_m = 0.341zF$. The transition rates depend on voltage and Ca^{2+} concentrations. Its dependence with voltage and parameters is provided in the Supporting information S1 File.

Calcium release: RyR

The calcium release current, through RyR, is like a diffusive current, but depending not only on the difference among c_{jsr} and c_d but also on the conductivity of RyR and, a non-deterministic feature of the model, the number of these proteins in the open state (O_{RyR}):

$$j_{RyR} = g_{rel} O_{RyR}(c_{jsr} - c_d) \quad (15)$$

In each CaRU we consider a cluster of $N_{RyR} = 40$ RyR, where each one of the receptors can be in one of the 4 possible states as shown in the second panel of Fig.1: O, for the open state; C is the closed state, while I1 and I2 are two inactivated/terminated states.

Their dynamics are treated stochastically as a function of transition rates k_{ss^*}, with s the previous state and s^* the state after the transition. At each time step, from the current configuration of states, the next configuration is randomly chosen following a Markov chain process using the RANMAR algorithm as uniformly random number generator used to obtain binomial numbers to decide how many RyR in the state s change to the different states s^*.

$k_{co} = k_{i2i1}$, and $k_{ci} = k_{oi}$ depend on calcium concentrations in junctional sarcoplasmic reticulum and dyadic junction at each time step with different cooperativities, while the rest of the rates are set as constants following the equalities $k_{ic} = k_{io}$ and $k_{oc} = k_{i1i2}$.

$$k_{co} = k_p \frac{2K_{jsr}^2 + c_{jsr}^2}{K_{jsr}^2 + c_{jsr}^2} \frac{c_d^2}{K_{oc}^2 + c_d^2} \tag{16}$$

$$k_{ci} = k_i \frac{2K_{jsr}^2 + c_{jsr}^2}{K_{jsr}^2 + c_{jsr}^2} \frac{c_d}{K_{in} + c_d} \tag{17}$$

where $K_{in} = 50\mu M$, $K_{oc} = 20\mu M$ and $K_{jsr} = 450\mu M$.

Calcium uptake: SERCA pump

The current given by the SERCA pump is thermodynamically limited. It is considered to depend only on Ca^{2+} concentrations in cytosol and network SR.

$$j_{SrCa} = \nu_{up} \frac{(c_i/K_i)^2 - (c_{sr}/K_{sr})^2}{1 + (c_i/K_i)^2 + (c_{sr}/K_{sr})^2} \tag{18}$$

where K_i and K_{sr} are half occupation binding constants, and ν_{up} the maximum uptake strength.

In the analysis of the paper regarding the effect of changes in SERCA in the calcium transient, we change the value of ν_{up}. This change mimics increases/decreases in the number of pumps present in each of the CaRUs. This is related to the number of pumps expressed in the SR membrane and should increase if SERCA therapy works properly.

Parameters of the rabbit model and its modified version

A full list of parameters of the rabbit model is provided in the appendix of the Supporting information S1 File. Furthermore, this appendix also includes the changes in the parameters of the modified rabbit model used in Fig. 2. This modification of the rabbit model allows us to show in the introduction that the effects of increasing the conductivity of LCC can depend a lot on the animal model. We must stress that we change the parameters of our rabbit model but not its structure. More specifically, our modified rabbit model has different buffers in order to change the effect on the level reached by calcium in the transient and a slightly reduced maximum SERCA uptake to mimic a slight reduction in its expression.

Results

We proceed to demostrate that a bi-dimensional general equilibrium approach provides the proper framework to understand and predict intracellular calcium levels at steady-state. We show that the actual homeoastatic calcium level observed in an in-silico rabbit ventricular model can be predicted using a dramatic reduction of dimensionality, where the general equilirium of thousands of variables is effectively, given the charactersitics of the problem, reduced into a general equilibrium of two variables, namely, the level of free calcium in the cytosol and the level of free calcium in the SR.

General equilibrirum

As described in the methods section, we consider a subcellular compartmental model of calcium handling, dividing the cell into Calcium Release Units (CaRUs), each incorporating a cluster of RyRs and of LCC, whose gating follows a Markov chain, solved stochastically. Let us denote the current of calcium that goes into the cell

through the LCC channels associated with the ith CaRU as j^i_{LCC}. The average flux of calcium entering the cell via LCC J_{LCC} (mol/s) is:

$$J_{LCC} = \frac{1}{N}\sum_i j^i_{LCC} \tag{19}$$

where N is the number of CaRUs in the cell. Integrating during the period T we obtain the total amount of calcium that enters/intrudes the cell during one beat:

$$\Delta Q_{in} = \int_0^T J_{LCC}\, dt. \tag{20}$$

We can define similarly the average flux of calcium that leaves/extrudes the cell via the Na-Ca exchanger J_{NCX} and the total amount of calcium that leaves the cell ΔQ_{out}.

$$J_{NCX} = \frac{1}{N}\sum_i j^i_{NCX}, \quad \Delta Q_{out} = \int_0^T J_{NCX}\, dt. \tag{21}$$

Notice that both ΔQ_{in} and ΔQ_{out} depend, in principle, on the value of the roughly one hundred thousand internal variables ϕ_i (number of open LCCs, amount of Ca attached to buffers, etc, at each of the different CaRUs) that define the state of the cell at the beginning of the beat. We assume that, despite the stochastic nature of LCC and RyR2 channels, average values are well-behaved. Being this the case, we can establish that the total amount of calcium Q^n_T at beat n follows the relation $Q^{n+1}_T = Q^n_T + \Delta Q^n_{in} - \Delta Q^n_{out}$ so that at steady state (ss) we have:

$$\Delta Q^{ss}_{in}(\phi_i) = \Delta Q^{ss}_{out}(\phi_i) \tag{22}$$

The total amount of calcium released via RyR2 from the SR to the cytosol, ΔQ_{rel}, and the total calcium uptaken by SERCA, ΔQ_{up}, can be equally defined from the average fluxes of all individual RyR clusters, J_{RyR}, and SERCA pumps, J_{SrCa}:

$$\Delta Q_{rel} = \int_0^T J_{RyR}\, dt \qquad \Delta Q_{up} = \int_0^T J_{SrCa}\, dt \tag{23}$$

In steady state, the amount of calcium in the SR must be constant, leading to

$$\Delta Q^{ss}_{rel}(\phi_i) = \Delta Q^{ss}_{up}(\phi_i) \tag{24}$$

As stated before, ventricular myocytes reproduce consistent average behavior. Therefore, fluxes in Eqs. (22), (24) depend on the relevant spatial average variables $\overline{\phi}_i$ (see the SM for the list of average variables which define our cell model) and not on their spatial distribution.

Except for average calcium concentrations, all the average quantities that define the state of the cell under voltage-clamped conditions have relaxation time scales which are shorter than the fastest pacing period reached. This typically goes from $T_{min} = 300 - 400$ ms in humans to $T_{min} = 150 - 200$ ms in rats. With this in mind, we notice that LCC, exchanger, SERCA and buffer characteristic time scales are typically faster than T_{min}. Recovery times of the RyR2 are probably around 100 ms, safely below T_{min} for most species.

Thus, we claim that it is possible to do a separation of time scales, such that the dynamics of the homeostatic process occurs in a slow manifold, where the dynamics of the fast variables slaves to that of the slow variables (or order parameters, in synergetic terminology [33]). We, thus, divide the variables into fast, ϕ_{fast}, and slow, ϕ_{slow}. The latter equilibrate in a time scale of several beats. At each individual beat, however, the

former attain their equilibrium values, that will depend on the state of the slow variables, so $\phi^n_{fast} = h(\phi^n_{slow})$. This leads us to the conclusion that the surface which determines homeostasis suffers a huge effective reduction of its dimensionality since memory is mainly eliminated by the external pacing. Flows in one beat are then determined only by the diastolic free SR concentration c_{sr} and cytosolic concentrations c_i, that act as slow variables, such that at steady state we have:

$$\Delta Q_{in}(c^{ss}_{sr}, c^{ss}_i) = \Delta Q_{out}(c^{ss}_{sr}, c^{ss}_i) \quad (25)$$

$$\Delta Q_{rel}(c^{ss}_{sr}, c^{ss}_i) = \Delta Q_{up}(c^{ss}_{sr}, c^{ss}_i) \quad (26)$$

These are two equilibrium conditions for two independent global average variables. If a steady state exists, it corresponds to the simultaneous fulfillment of the two global equilibrium conditions. Alternatively, the solution to these equations may either not exist or, if it does, be unstable, corresponding to, for instance, alternans or chaotic behavior. In this paper, we address the first scenario with a stable fixed point.

Validation

From Eqs. (25), (26) we can predict the average diastolic calcium level at steady-state from measurements away from steady-state. Figs 3 and 4 sketch the basic procedure to predict the steady state from single beat measurements. We simulate the evolution of calcium concentrations, c_i and c_{sr}, during one single beat, taking different initial calcium diastolic values (i.e. different initial conditions), with all the local variables unrelated to calcium concentrations set initially at their fast-equilibrium approximation. From this evolution we can compute how much calcium leaves the SR, ΔQ_{rel}, or enters the SR, ΔQ_{up}, during this beat, and repeat the calculation for a different initial condition. This gives new values of ΔQ_{rel} and ΔQ_{up}. If we repeat this procedure for multiple combinations of initial values of c_i and c_{sr} we can reconstruct the dependence of the currents with the diastolic calcium concentrations. We obtain the functions $\Delta Q_{rel}(c_{sr}, c_i)$ and $\Delta Q_{up}(c_{sr}, c_i)$, which are nothing else than surfaces in a diastolic calcium concentration space as shown in Fig. 3.

Fig 3. Schematics of the procedure to reconstruct one of the nullclines of the system The nullcline corresponds to the partial equilibrium where the intake of calcium into the SR equals its release. The main central graph reproduces total release ΔQ_{rel} and uptake ΔQ_{up} as a function of the initial free concentrations in the cytosol $c_i(t = 0)$ and SR $c_{SR}(t = 0)$. The nullcline is determined by the line where both surfaces cross. For each initial conditions, one single transient is simulated and the release J_{RyR} and uptake J_{SrCa} computed and shown in the upper graphs. The integrated values are indicated in the bar graph below and then placed as elements of the surface. The whole surface is constructed by reproducing this procedure with multiple different initial calcium concentrations where all other initial variables are in their fast equilibrium approximation.

The line where both surfaces cross (see $\Delta Q_{rel} = \Delta Q_{up}$ in Fig. 3), or g-nullcline, fulfills the partial equilibrium indicated by Eq. (25). To obtain the partial equilibrium given by Eq. (26) we construct the surfaces for $\Delta Q_{in}(c_{sr}, c_i)$ and $\Delta Q_{out}(c_{sr}, c_i)$ using the same procedure indicated in Fig. 3. The line where they cross is the f-nullcline, which represents the equilibrium condition that at steady state the same amount of calcium that enters the cell must leave it. The point where both nullclines intersect gives us the concentration of diastolic calcium which fulfills both equilibrium conditions. This sets the steady state, i.e., it predicts the diastolic homeostatic calcium level and its internal distribution between the SR and cytosol of the cell.

Fig 4. General equilibrium. Prediction of steady-state from the nullclines crossing. Panel (1): The first two surfaces indicate the total amount of calcium entering ΔQ_{in} and leaving ΔQ_{out} the cell, computed following the same procedure explained in Fig. 3. Below we compute the surfaces corresponding to release and uptake of calcium from the SR. On the right, we plot the two nullclines that correspond to the crossing of the previous surfaces. The f-nullcline is the set of initial c_i and c_{sr} where $\Delta Q_{in} = \Delta Q_{out}$ while the g-nullcline corresponds to the crossing between release ΔQ_{rel} and uptake ΔQ_{up}. The point where both nullclines cross gives the steady state of the system (c_i, c_{SR}) where concentrations return to the same pre-systolic values after a stimulation. Panel (2): Steady state from single beat measurements at 2 Hz described in the top panel with modification of the rabbit model where the conductivity of LCC is increased. The prediction of the steady state obtained from the global equilibrium as a function of the LCC conductivity fits perfectly the computed steady-state obtained after letting the system evolve for 100 beats.

We have checked that the prediction given by the crossing of the nullclines agrees perfectly with the calcium concentration values obtained letting the system evolve to steady-state (bottom panel of Fig. 4).This agreement confirms the validity of the reduction in dimensionality. This reduction is not at all trivial. It comes from the fact that average values are not very sensible to the inherent noise of the system in ventricle myocytes and that the processes involved in calcium handling have time scales which are faster than the pacing period. Regarding calcium homeostasis, each period of the system provides a global reset of the fast variables leaving only the slow concentration variables in play. We provide further information regarding this point in the Supporting information S1 File where we show that the total calcium concentrations in the cell and the SR can also be treated as the key analytical variables instead of free calcium concnetrations. The reason is that free calcium concentrations and total calcium concentrations can be related one-to-one, in a general equilibrium framework, using the fast-buffering approximation.

Discussion

Our key result has deep implications for the analysis of cardiomyocyte contractibility. We can use this framework to infer how the cell behavior will be modified upon a change in channel properties or the increase of buffers levels. More specficially, we can use the insights from bi-dimensional general equilibrium problems from other fields and understand the anti-intuitive response of cells to changes at the channel level, as described in the introduction. We will focus our discussion on changes in SERCA function given its possible relevance to understand gene therapy failure. We will show that, in terms of shocks, as they are normally called in the literature, a change of SERCA strength is actually a double shock. With this realization in mind we proceed to unveil and discuss a physiological mechanism for SERCA gene therapy failure where, even in the case of SERCA improved function, calcium transient and contractibility are not improved.

General shocks

Analysis of stability based on partial equilibrium conditions is common in other fields, as macroeconomics. In fact, this framework can be mapped one-to-one to the Investment-Saving, Liquidity preference-Money supply (IS-LM) model of macroeconomics developed by J. Hicks [2] as an explanation of Keynes general theory

of Employment, Interest and Money [34]. In the IS-LM, the steady-state of a large complex closed economy is defined by its ouput (average GDP per capita) and by the average interest rate, just like in our case we define our steady state by two variables, the average calcium concentration in the cytosol and the SR. Equally, the general equilibrium conditions that must be met are two. First, Investment has to balance Saving, leading to the IS curve, equal to our f-nullcline. The equivalent of our g-nullcline involves the interest rates and output for which the money market is in equilibrium.

There, a shock is a sudden change in the curves that determine equilibrium. In our case, a change in the conductivity or the property of a particular receptor or the strength of SERCA/NCX is a shock that changes the four surfaces corresponding to the four fluxes. If the shock were only to affect strongly the surfaces related to the release and uptake of calcium from the SR (as sketched in the first panel of Fig. 5), then just the g-nullcline would shift position. From this shift and the slope of the f-nullcline we can predict the effect of the shock. For example, if the uptake of calcium is raised (increasing the ΔQ_{up} surface) then the g-nullcline will shift down. Given that, in this example, the slope of the f-nullcline is negative, the downward shift of the g-nullcline will move the crossing of the two nullclines, and the steady state, to higher c_{sr} and lower c_i.

Fig 5. Shocks in general equilibrium models. Change in SERCA uptake is a two-nullcline shock Panel (1): We show a hypothetical change in the cell that only affects one of the four surfaces. This produces a change in one of the nullclines. As an example, we pick an increase of the ΔQ_{up} surface. This leads to a shift of the g-nullcline to the right compared with the previous case, resulting in a lower diastolic level in the cytosol but larger in the SR. Panel (2): Effect of changing the maximum uptake of the SERCA pump from 0.15 μ M/ms to 0.3 μ M/ms in our rabbit model. Increasing the function of SERCA does not only affect the g-nullcline, expected since the uptake is larger, but also affects how well the exchanger works shifting also the f-nullcline to the right. The end result is similar to the previous case.

However, as we proceed to describe in the next sections, changes in key functioning elements of calcium homeostasis normally affect two or all four of the surfaces. To be specific, we are going to consider a change in SERCA function.

Consequences of shocks

We aim to understand how an increase in SERCA function affects the homeostatic state and whether it systematically leads to improved calcium transients and contraction. We will model this increase in SERCA function with an increase in its maximum uptake rate v_{up} and proceed to answer a simple question. Will a change of SERCA function always lead to larger/broader calcium transients?

Change in SERCA function is a double shock

We observe that changes in v_{up} affect not only the surface directly related with the uptake ΔQ_{up}, but also ΔQ_{out}. Thus, a change in SERCA function is a double shock, since it changes two nullclines, as shown in the bottom panel of Fig. 5. The reason is rather intuitive. A change in the uptake does not have a strong effect in the behavior of the LCC channels and hardly changes the release, but a more efficient SERCA reduces quickly cytosolic calcium levels, which reduces the efficiency of the exchanger. The effect is that the shock associated with larger uptake moves both nullclines to the right. Given the structure of the nullclines, shown in Fig. 5, where the f-nullcline has a negative slope while that of the g-nullcline is positive, it is thus straightforward that they will cross at a higher level of SR. In fact, we observe that the level of calcium in the SR

increases monotonically, while the level in the cytosol decreases also monotonically (left of the first panel of Fig. 6). In the Supporting information S1 File, we show that the total amount of calcium in the cell, this is, the sum of calcium in the cytosol and SR, increases slightly as we increase the SERCA uptake given that the increase in calcium in the SR compensates a reduction of calcium levels in the cytosol. While the increase in SR load depends on the slope of the nullclines, whether pre-systolic calcium in the cytosol increases or decreases depends on how far both nullclines move with the shock. Thus, the fact that the nullclines cross at lower cytosolic calcium is not a structural result but it depends on the particulars of the system.

Fig 6. Homeostatic response of increasing SERCA uptake with normal and low RyR channel conductivity. Panel (1): Dependence of pre-systolic values of free calcium concentrations in the SR and in the cytosol at steady state with maximum uptake of SERCA pump v_{up} in the rabbit model. On the right, the relative increase of calcium during the calcium transient as a function as a function of the maximum SERCA uptake ν_{up}. We take 100% to be the trasnient with the standard $\nu_{up} = 0.5$ μM/ms. Panel (2): We present the same graphs as in the first panel but for a cell where the single channel conductivity of the RyR has been reduced. In this situation, the calcium transient is always lower than before and it does not improve as the uptake of SERCA is larger.

The shift of the nullclines due to the increase in SERCA function is a quantification of how SERCA interacts with the exchanger and, indirectly, via changes in the release, with the LCC. A faster SERCA uptake reduces the ability of the exchanger to extrude calcium since SERCA pushes down calcium in the cytosol faster during diastole, making the gradient of calcium between the cytosol and extracellular space larger (see Fig. 7). Given that the exchanger does not work as well with a large gradient in calcium, one would think that it would extrude less calcium. However, this cannot be the case. Since ΔQ_{in} is a rather flat surface, calcium entering via LCC, as SERCA increases, remains roughly unchanged. Thus, to reach equilibrium, calcium extruded by the exchanger has to remain almost constant too. The only possibility is that the system reaches a different homeostatic equilibrium in which the release and calcium transient adapt so that the exchanger can extrude the same as it did before the shock.

Fig 7. Schematics of possible SERCA gene therapy failure. Schematics of how SERCA gene therapy may fail in certain cells. In thick boxes steps that happen in all models. The filled-in arrows linking boxes indicate a necessary consequence. For example, a sudden increase in maximum SERCA uptake does not change initially the LCC or the release but it affects the uptake of calcium to the SR and the NCX function. This necessarily leads to a state of calcium unbalance that must be rebalanced again. Without boxes, we show steps that are particular of this failure mechanism. Similarly, non-filled arrows represent possible outcomes that depend on the model and lead to smaller transients. In a thin box, a step which is general and particular at the same time. As indicated in the thin box, homeostasis will always fix and rebalance the system, however, the particulars of how this is done are not universal. They depend on the nullcline structure and reaction to shocks. It is not universal that nullclines will dictate an increase in both the cytosol and the SR. Actually, in a healthy rabbit, it loads the cell by increasing a lot the SR while diminishing cytosolic calcium levels. In this failure scheme, it loads both.

The resulting changes in the calcium transient when we increase the maximum SERCA uptake at steady-state are summarized on the right graph of the first panel in Figure 6. The transient amplitude must change if diastolic cytosolic calcium decreases.

We observe that the peak of calcium transient barely changes, but given that the minimum of the transient decreases, the amplitude raises appreciably. The end result is that in this animal model, a higher v_{up} increases the contractibility of the cell, given the larger transient.

Physiological mechanism for SERCA gene therapy failure

Now we aim to answer a simple question. Will a change of SERCA function always lead to larger/broader calcium transients? For that, we will reproduce a possible malfunction. Given that there are calcium-binding proteins which affect both SERCA and RyR [19], we consider a rabbit cell where the conductivity of the RyR is reduced without changes in the exchanger or the LCC. The details of the rabbit cell with reduced RyR activity are explained in the SM where we show that the slopes of both nullclines are still the same as in the original rabbit model. However, as the second panel of Fig. 6 shows, there are crucial differences with the wild-type scenario, mainly that the calcium transient is actually reduced leading to lower contraction when SERCA maximum uptake is increased.

Given that the structure of the nullcline is the same, increasing the SERCA uptake in the RyR2 modified rabbit cell leads to higher diastolic SR load (see Fig. 7). However, as shown in the left graph of the second panel in Fig. 6, higher v_{up} leads to an increase of the diastolic cytosolic calcium. The reason is that, in this case, the shift in the f-nullcline is larger than in the g-nullcline (see SM for details). Given that, now the exchanger works more efficiently. On the other hand, the surface ΔQ_{in} is very flat, so the calcium influx remains almost constant. This means that the exchanger has to extrude roughly the same amount of calcium no matter what the SERCA uptake is. This directly leads to a decrease of the transient, as shown at the graph on the right of the second panel in Fig. 6. Actually, both the minimum is increased and the maximum is reduced at steady-state, leading to a strongly reduced transient, exactly the opposite of the wild-type case.

The sketch of the physiological mechanism for SERCA gene therapy failure is described in detail in Fig. 7 where a clear distinction is made between the conclusions of our analysis which would hold for any type of cell and those which are dependent on the model and the specific properties of the general equilibrium achieved. Upon an increase in SERCA uptake, all cells will not, initially, change its calcium intake via LCC and release via RyR. However, the NCX will be affected by a larger gradient in calcium leading to a reduction in its function. The system is no longer in equilibrium and must rebalance loading calcium. This change in calcium levels affects all elements of calcium handling, including those that were not initially affected: intake and release. The specifics of how this increase in calcium is distributed depends on the particulars of the general equilibrium state of the cell. The slope of the nullclines will determine if SR will be more loaded as it is normally the case. The effect of the shock on the nullclines will determine whether cytosolic calcium is increased, because the cell will load until NCX function is restored thanks to a reduced gradient, or decreased, in case the NCX function is restored thanks to a larger transient provided by a more loaded SR. Both are perfectly possible outcomes of the shifts in the nullclines given the shock given to the cell.

Conclusion

Detailed models of calcium handling have been able to reproduce spatiotemporally complex behavior as discordant alternans [35] or calcium waves [36, 37], and have been used, for instance, to understand the onset of alternans as a synchronization

transition [38]. Surprisingly given the complexity of the dynamics, the equilibrium conditions can be obtained using, as in very simple models, average variables and balance of fluxes in the cytosol and the SR. This result is not trivial. It requires that all internal variables, except cytosolic and SR calcium, equilibrate at the time scale of the pacing period. Also, that all CaRUs behave on average as the averaged variable, to prevent the appearance of intracellular inhomogeneities with different behavior.

As we have discussed earlier in this paper, this dimensionality reduction is not uncommon in other complex systems. We understand the equilibrium point as satisfying two partial equilibrium conditions: calcium in and out of the cell and of the SR must balance. We can then use this description to understand the effects of shocks, i.e., changes in parameters that result in shifts in the curves denoting the partial equilibrium conditions. We observe that the effect of the shocks can be very different depending on the form of these curves. This is, the same recipe may have very different outcomes depending on the state of the system. In our ventricular model, these shocks may produce counterintuitive results. As, for instance, a decrease in SR calcium concentration as the strength of the LCC channels is increased. This can be well understood with the shifts in the partial equilibrium curves. Clearly, a further investigation of what determines the slope of the curves and how they depend on species or underlying pathologies should be undertaken.

Another relevant example is the effect of a change in SERCA. Upregulation of SERCA gene expression, or SERCA gene therapy, has been used to treat patients with heart failure. Even if this therapy is often successful, in some occasions it does not seem to work [22, 23]. From our results, one could think of a possible explanation as sketched in Fig. 7. Under some modifications on the parameters, an increase of SERCA strength does not lead to an increase in the cytosolic calcium transient, but rather the opposite. This is clearly an in-silico failure of SERCA therapy due to how the cell reacts to the double shock that the changes in SERCA represent. We have thus unveiled a possible physiological mechanism for SERCA therapy failure and how its success or failure depends on the basic structure and movement of the nullclines determining homeostatic steady-state upon changes in SERCA function.

References

1. Munasinghe M. Making economic growth more sustainable. Ecological Economics. 1995;15(2):121–124.

2. Hicks JR. Mr. Keynes and the" classics"; a suggested interpretation. Econometrica: journal of the Econometric Society. 1937;p. 147–159.

3. Bers D. Excitation-contraction coupling and cardiac contractile force. vol. 237. Springer Science & Business Media; 2001.

4. Endoh M. Force–frequency relationship in intact mammalian ventricular myocardium: physiological and pathophysiological relevance. European journal of pharmacology. 2004;500(1-3):73–86.

5. Gwathmey J, Slawsky M, Hajjar R, Briggs G, Morgan J. Role of intracellular calcium handling in force-interval relationships of human ventricular myocardium. The Journal of clinical investigation. 1990;85(5):1599–1613.

6. Janssen PM, Periasamy M. Determinants of frequency-dependent contraction and relaxation of mammalian myocardium. Journal of molecular and cellular cardiology. 2007;43(5):523–531.

7. Antoons G, Mubagwa K, Nevelsteen I, Sipido KR. Mechanisms underlying the frequency dependence of contraction and [Ca2+] i transients in mouse ventricular myocytes. The Journal of physiology. 2002;543(3):889–898.

8. Georgakopoulos D, Kass DA. Minimal force-frequency modulation of inotropy and relaxation of in situ murine heart. The Journal of Physiology. 2001;534(2):535–545.

9. Bers DM. Calcium fluxes involved in control of cardiac myocyte contraction. Circulation research. 2000;87(4):275–281.

10. Gattoni S, Røe ÅT, Frisk M, Louch WE, Niederer SA, Smith NP. The calcium–frequency response in the rat ventricular myocyte: an experimental and modelling study. The Journal of physiology. 2016;594(15):4193–4224.

11. Maier LS, Bers DM, Pieske B. Differences in Ca2+-handling and sarcoplasmic reticulum Ca2+-content in isolated rat and rabbit myocardium. Journal of molecular and cellular cardiology. 2000;32(12):2249–2258.

12. Eisner D, Bode E, Venetucci L, Trafford A. Calcium flux balance in the heart. Journal of molecular and cellular cardiology. 2013;58:110–117.

13. Lugo CA, Cantalapiedra IR, Peñaranda A, Hove-Madsen L, Echebarria B. Are SR Ca content fluctuations or SR refractoriness the key to atrial cardiac alternans?: insights from a human atrial model. American Journal of Physiology-Heart and Circulatory Physiology. 2014;306(11):H1540–H1552.

14. Eisner DA, Caldwell JL, Kistamás K, Trafford AW. Calcium and excitation-contraction coupling in the heart. Circulation research. 2017;121(2):181–195.

15. Landstrom AP, Dobrev D, Wehrens XH. Calcium signaling and cardiac arrhythmias. Circulation research. 2017;120(12):1969–1993.

16. Němec J, Kim JJ, Salama G. The link between abnormal calcium handling and electrical instability in acquired long QT syndrome–does calcium precipitate arrhythmic storms? Progress in biophysics and molecular biology. 2016;120(1-3):210–221.

17. Alvarez-Lacalle E, Cantalapiedra IR, Peñaranda A, Cinca J, Hove-Madsen L, Echebarria B. Dependency of calcium alternans on ryanodine receptor refractoriness. PloS one. 2013;8(2):e55042.

18. Chamberlain K, Riyad JM, Weber T. Cardiac gene therapy with adeno-associated virus-based vectors. Current opinion in cardiology. 2017;.

19. Gorski PA, Ceholski DK, Hajjar RJ. Altered myocardial calcium cycling and energetics in heart failure-a rational approach for disease treatment. Cell metabolism. 2015;21(2):183–194.

20. Samuel T, Rosenberry R, Lee S, Pan Z. Correcting Calcium Dysregulation in Chronic Heart Failure Using SERCA2a Gene Therapy. International journal of molecular sciences. 2018;19(4):1086.

21. Jaski BE, Jessup ML, Mancini DM, Cappola TP, Pauly DF, Greenberg B, et al. Calcium upregulation by percutaneous administration of gene therapy in cardiac disease (CUPID Trial), a first-in-human phase 1/2 clinical trial. Journal of cardiac failure. 2009;15(3):171–181.

22. Jessup M, Greenberg B, Mancini D, Cappola T, Pauly DF, Jaski B, et al. Calcium upregulation by percutaneous administration of gene therapy in cardiac disease (CUPID) a phase 2 trial of intracoronary gene therapy of sarcoplasmic reticulum Ca2+-ATPase in patients with advanced heart failure. Circulation. 2011;124(3):304–313.

23. Hulot JS, Ishikawa K, Hajjar RJ. Gene therapy for the treatment of heart failure: promise postponed. European heart journal. 2016;37(21):1651–1658.

24. Hamilton S, Terentyev D. Altered Intracellular Calcium Homeostasis and Arrhythmogenesis in the Aged Heart. International journal of molecular sciences. 2019;20(10):2386.

25. Trafford A, Diaz M, Eisner D. Coordinated control of cell Ca2+ loading and triggered release from the sarcoplasmic reticulum underlies the rapid inotropic response to increased L-type Ca2+ current. Circulation research. 2001;88(2):195–201.

26. Mahajan A, Shiferaw Y, Sato D, Baher A, Olcese R, Xie LH, et al. A rabbit ventricular action potential model replicating cardiac dynamics at rapid heart rates. Biophysical journal. 2008;94(2):392–410.

27. Galice S, Xie Y, Yang Y, Sato D, Bers DM. Size matters: Ryanodine receptor cluster size affects arrhythmogenic sarcoplasmic reticulum calcium release. Journal of the American Heart Association. 2018;7(13):e008724.

28. Rog-Zielinska EA, Johnston CM, O'Toole ET, Morphew M, Hoenger A, Kohl P. Electron tomography of rabbit cardiomyocyte three-dimensional ultrastructure. Progress in biophysics and molecular biology. 2016;121(2):77–84.

29. Macquaide N, Tuan HTM, Hotta Ji, Sempels W, Lenaerts I, Holemans P, et al. Ryanodine receptor cluster fragmentation and redistribution in persistent atrial fibrillation enhance calcium release. Cardiovascular research. 2015;108(3):387–398.

30. Soeller C. Ryanodine receptor cluster size sets the tone in cerebral smooth muscle. Proceedings of the National Academy of Sciences. 2018;115(41):10195–10197.

31. Shannon TR, Wang F, Puglisi J, Weber C, Bers DM. A mathematical treatment of integrated Ca dynamics within the ventricular myocyte. Biophysical journal. 2004;87(5):3351–3371.

32. Bassani J, Bassani RA, Bers DM. Relaxation in rabbit and rat cardiac cells: species-dependent differences in cellular mechanisms. The Journal of physiology. 1994;476(2):279–293.

33. Haken H. Synergetics: introduction and advanced topics. Springer Science & Business Media; 2013.

34. Keynes JM. The general theory of employment, interest, and money. Springer; 2018.

35. Sato D, Shiferaw Y, Garfinkel A, Weiss JN, Qu Z, Karma A. Spatially discordant alternans in cardiac tissue: role of calcium cycling. Circulation research. 2006;99(5):520–527.

36. Shiferaw Y, Aistrup GL, Wasserstrom JA. Intracellular Ca2+ waves, afterdepolarizations, and triggered arrhythmias. Oxford University Press; 2012.

37. Izu LT, Xie Y, Sato D, Bányász T, Chen-Izu Y. Ca2+ waves in the heart. Journal of molecular and cellular cardiology. 2013;58:118–124.

38. Alvarez-Lacalle E, Echebarria B, Spalding J, Shiferaw Y. Calcium alternans is due to an order-disorder phase transition in cardiac cells. Physical review letters. 2015;114(10):108101.

S1 File. Supporting information file with appendix In this supplemental information file, we develope the nullcline analysis, mentioned in the results section, using total calcium concentrations in the cell instead of free calcium concentrations. We also provide additional details on how SERCA uptake changes affect cell behavior concerning the physiological mechanism for SERCA gene therapy failure, as indicated in the discussion section. This supplemental file also includes an appendix with tables of the different parameters used in the models.

Acknowledgments

Financial support was provided by the Fundació La Marató de TV3, under grant number 20151110, and from the Spanish Ministerio de Economía y Competitividad (MINECO) under grants number SAF2017-88019-C3-2-R and PGC2018-095456-B-I00. Support for YS was provided by NHLBI grant HL R01-119095. We want to thank L.Hove-Madsen from fruitful discussion

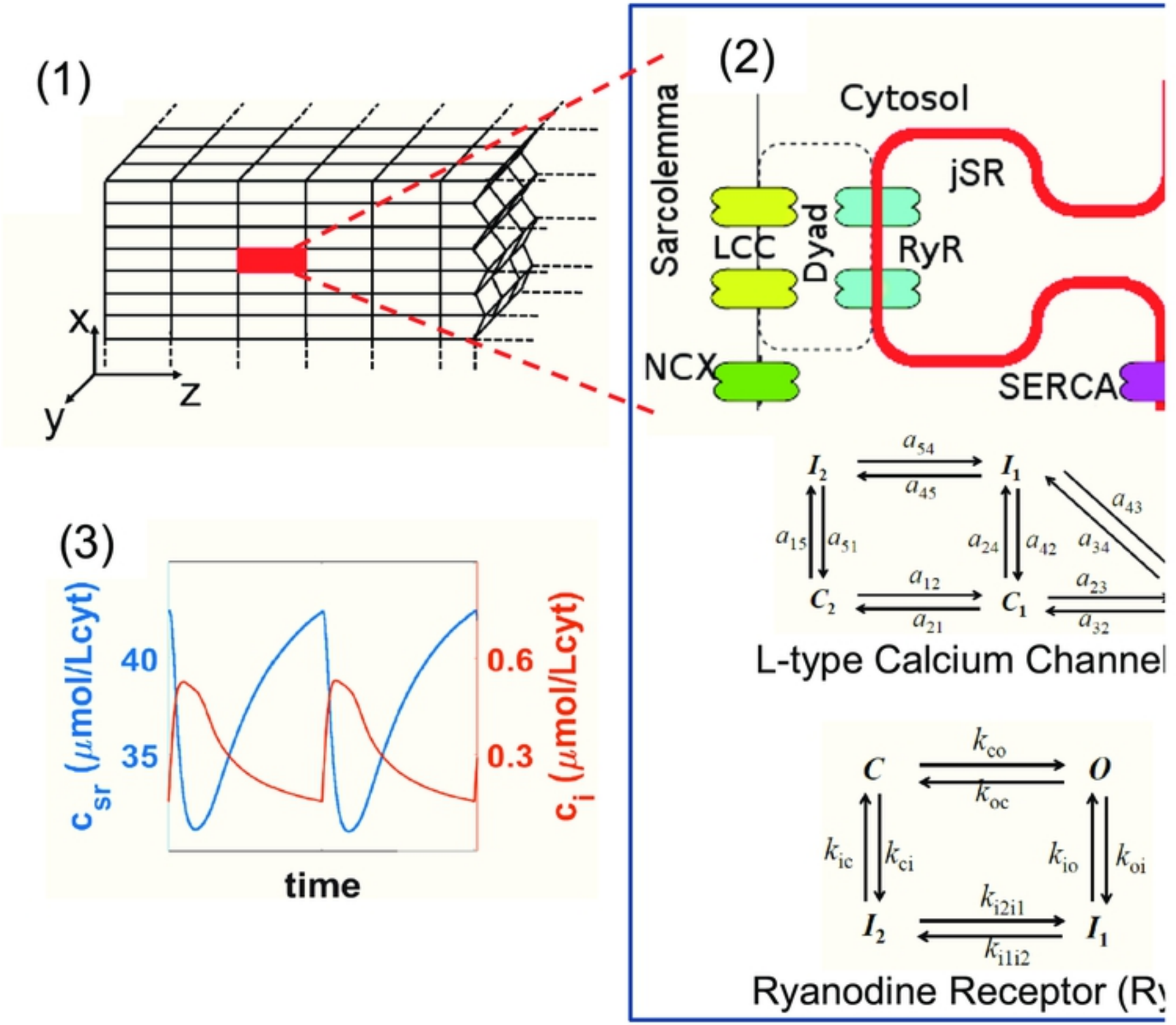
(1)
x
z
y
(2)
Cytosol
Sarcolemma
jSR
LCC
Dyad
RyR
NCX
SERCA
I_2
I_1
C_2
C_1
a_{54}
a_{45}
a_{43}
a_{15}
a_{51}
a_{24}
a_{42}
a_{34}
a_{12}
a_{21}
a_{23}
a_{32}
L-type Calcium Channel
(3)
40
35
0.6
0.3
c_{sr} (μmol/Lcyt)
c_i (μmol/Lcyt)
time
C
O
I_2
I_1
k_{co}
k_{oc}
k_{ic}
k_{ci}
k_{io}
k_{oi}
k_{i2i1}
k_{i1i2}
Ryanodine Receptor (R

Figure 1

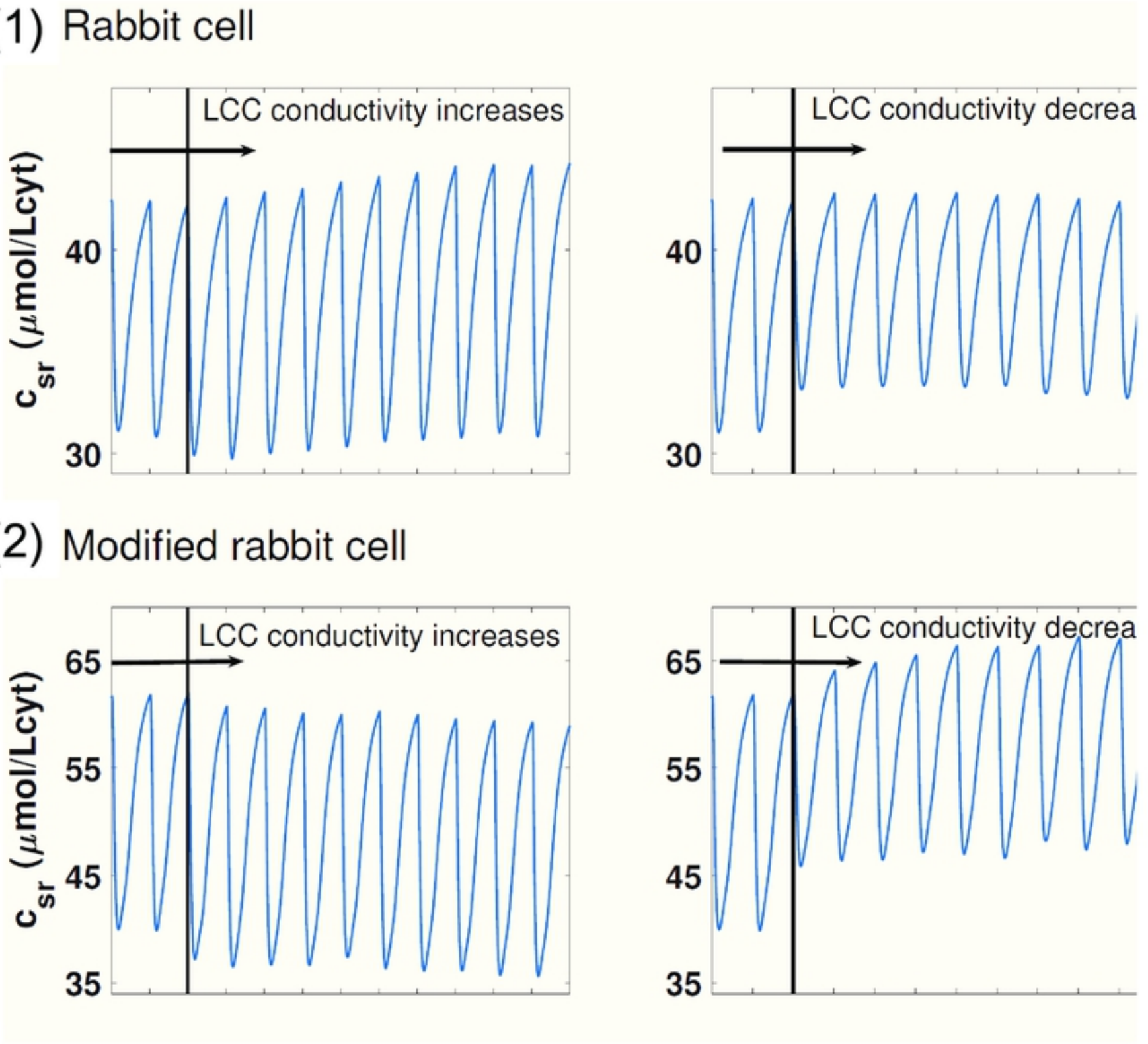
(1) Rabbit cell
LCC conductivity increases
LCC conductivity decrea
c_{sr} (μmol/Lcyt)
40
30
(2) Modified rabbit cell
LCC conductivity increases
LCC conductivity decrea
65
55
45
35

Figure 2

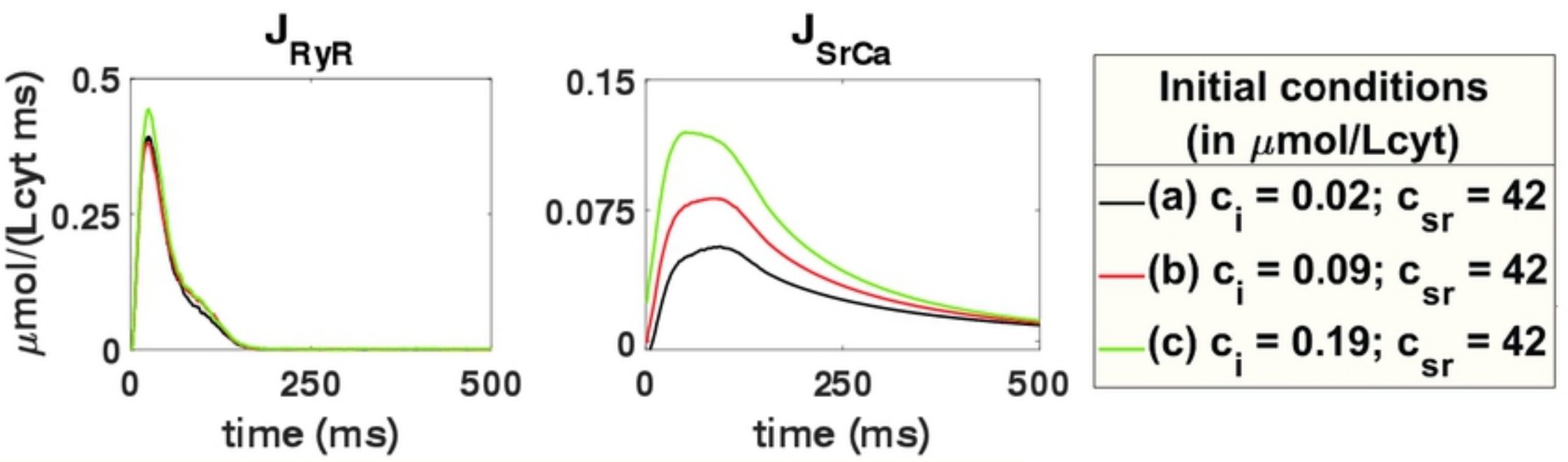
J_RyR
J_SrCa
μmol/(Lcyt ms)
0.5
0.25
0
0.15
0.075
0
0
250
500
time (ms)
Initial conditions
(in μmol/Lcyt)
(a) c_i = 0.02; c_sr = 42
(b) c_i = 0.09; c_sr = 42
(c) c_i = 0.19; c_sr = 42
ΔQ_rel
Tagged ΔQ_rel
ΔQ_up
Tagged ΔQ_up
1.6
fmol
0.8
0
0.4
0.2
c_i
20
40
60
c_sr
(a)
(b)
(c)
1
0.5
0
(a)
(b)
(c)

Figure 3

(1) Currents surfaces and nullclines

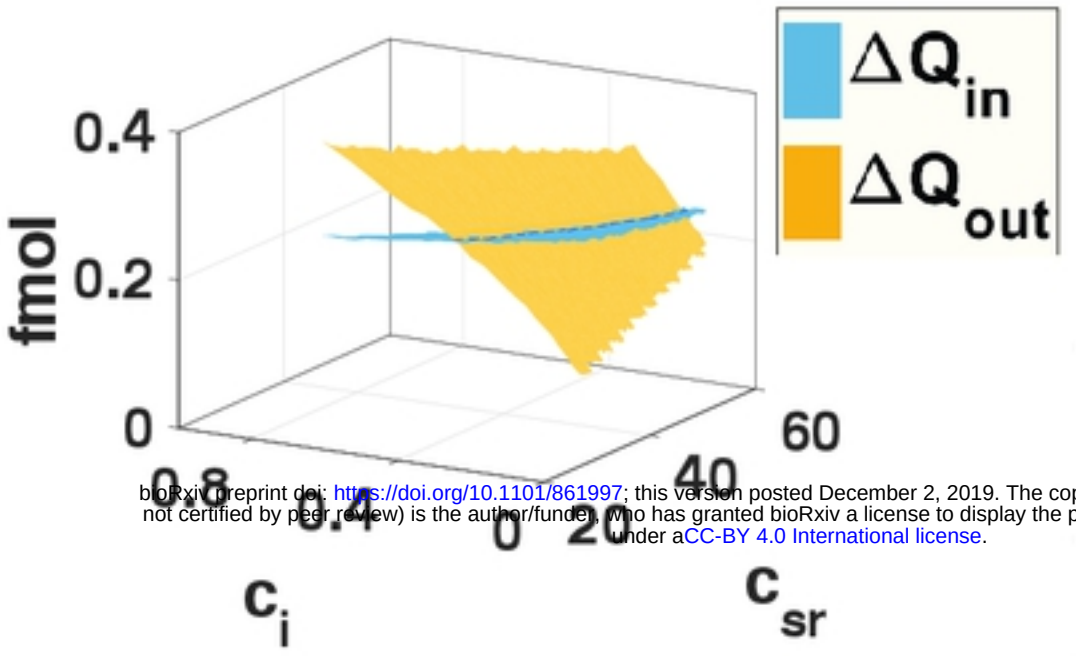

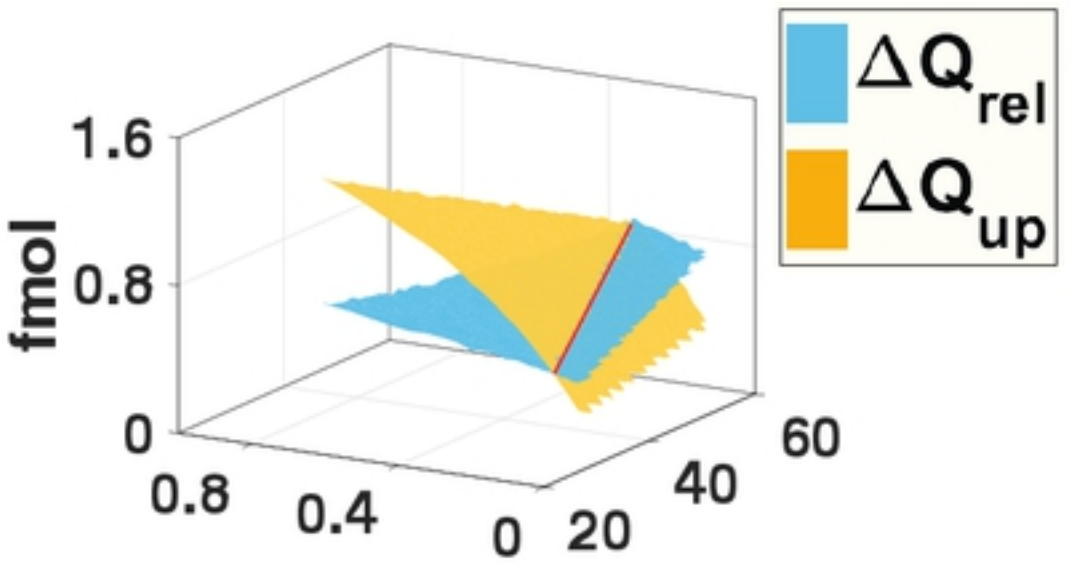

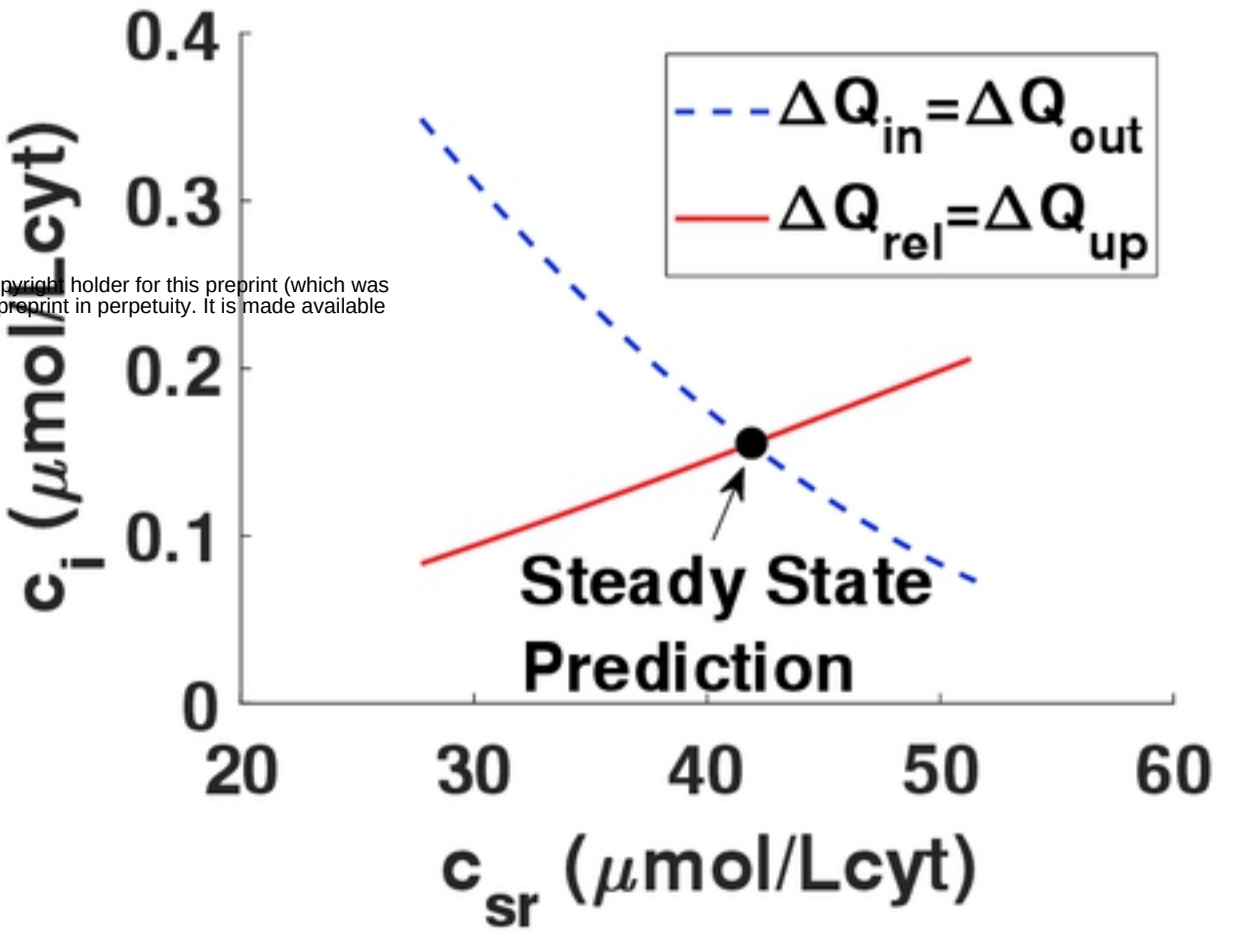

(2) Prediction vs. Steady State

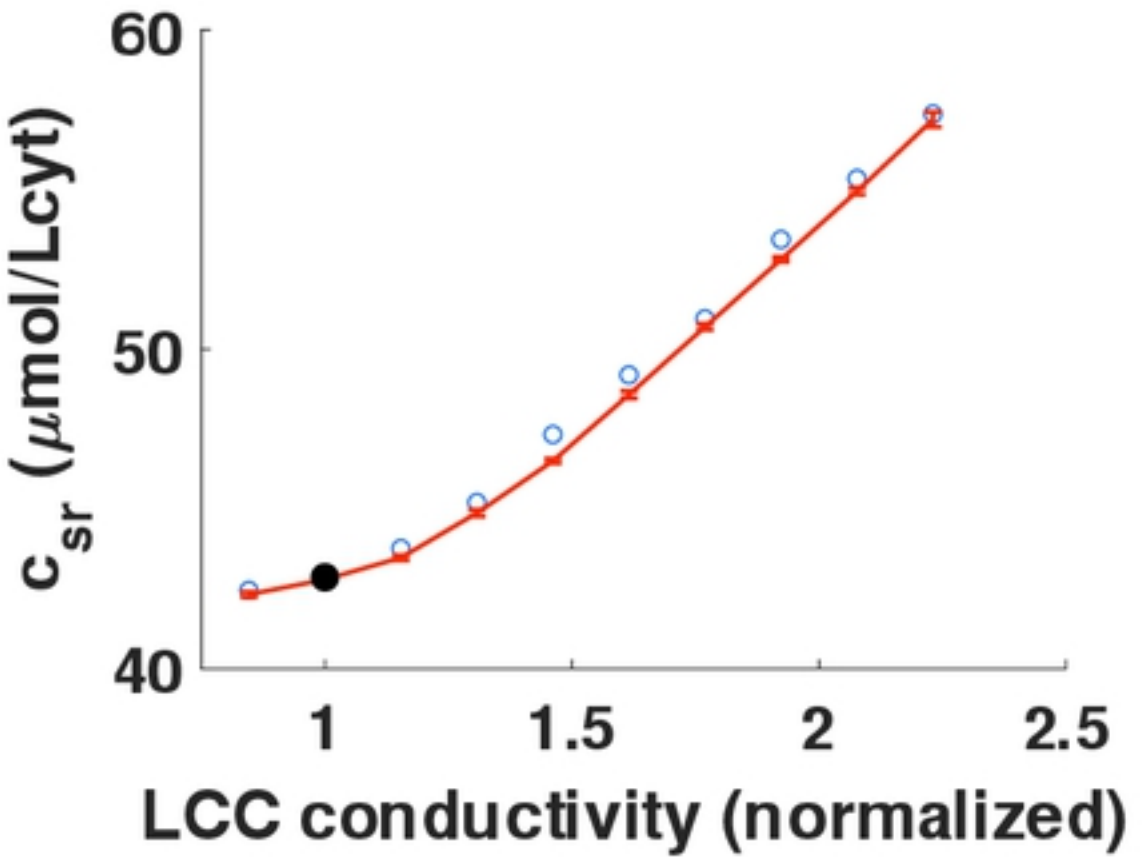

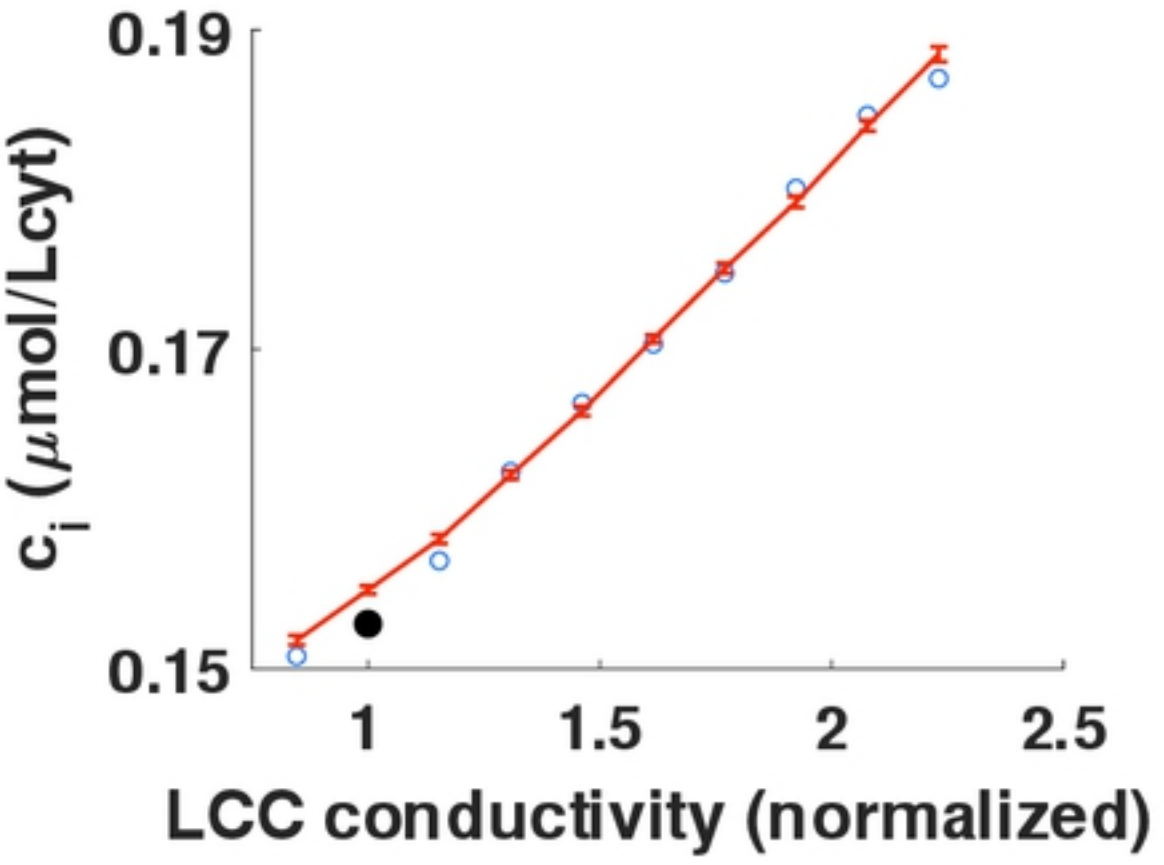

Figure 4

(1) Mechanics of a single shock

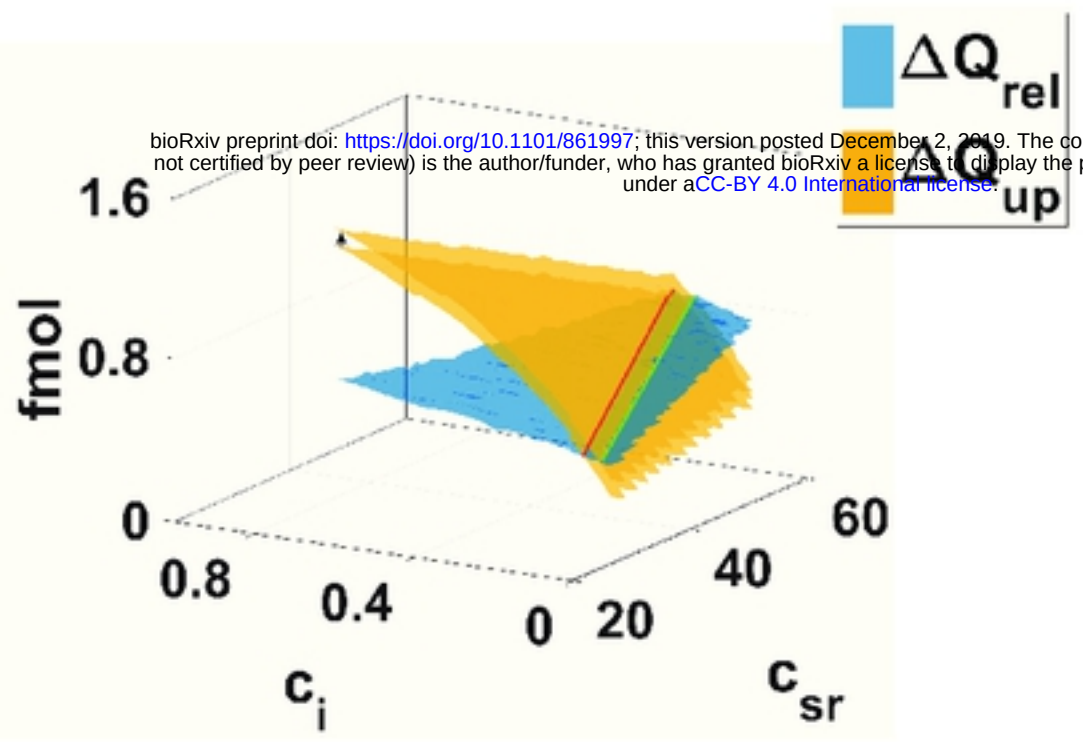

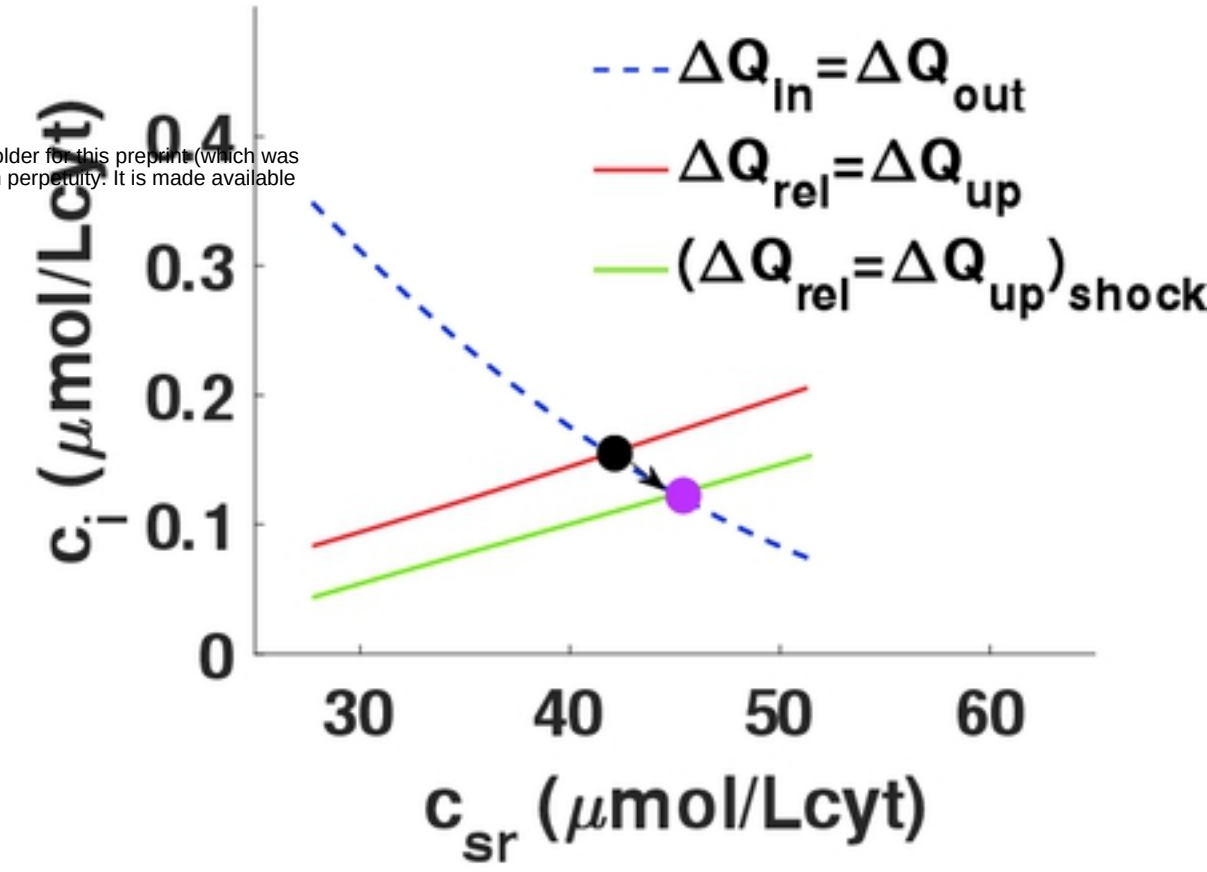

(2) Increasing SERCA uptake actually leads to a double shock

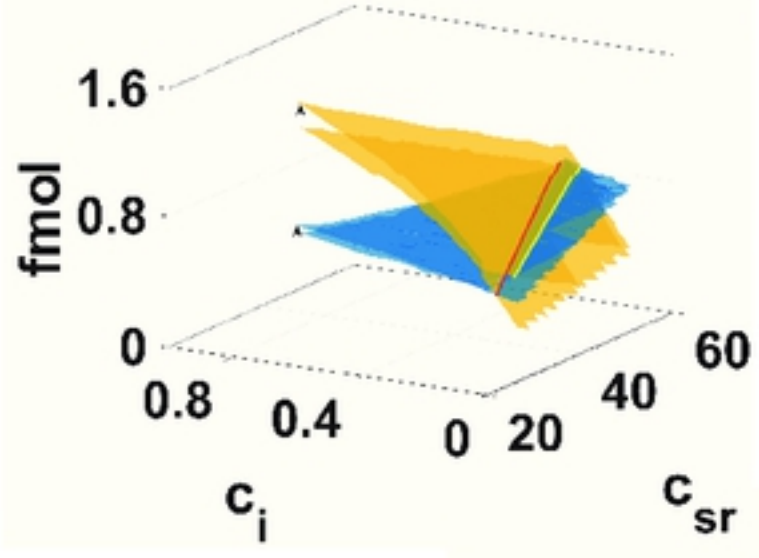

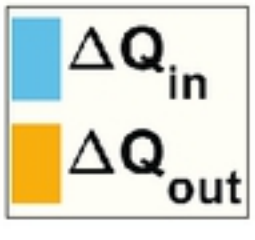

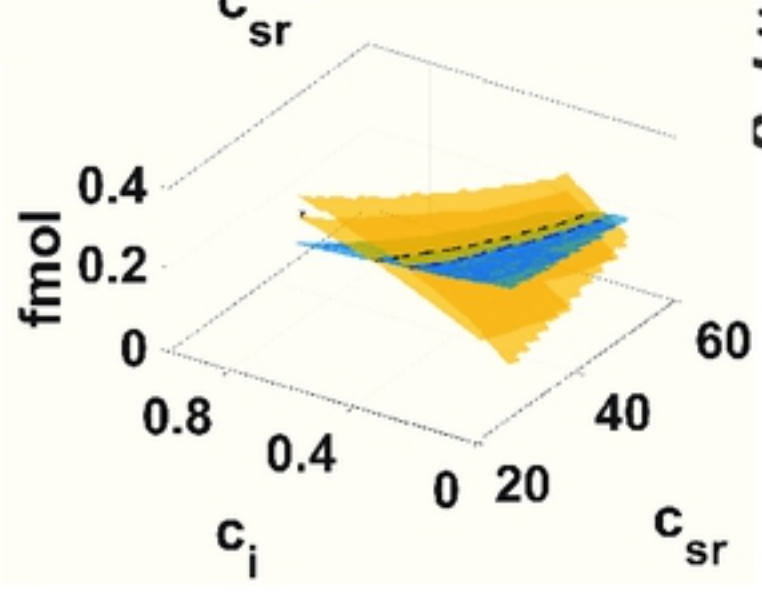

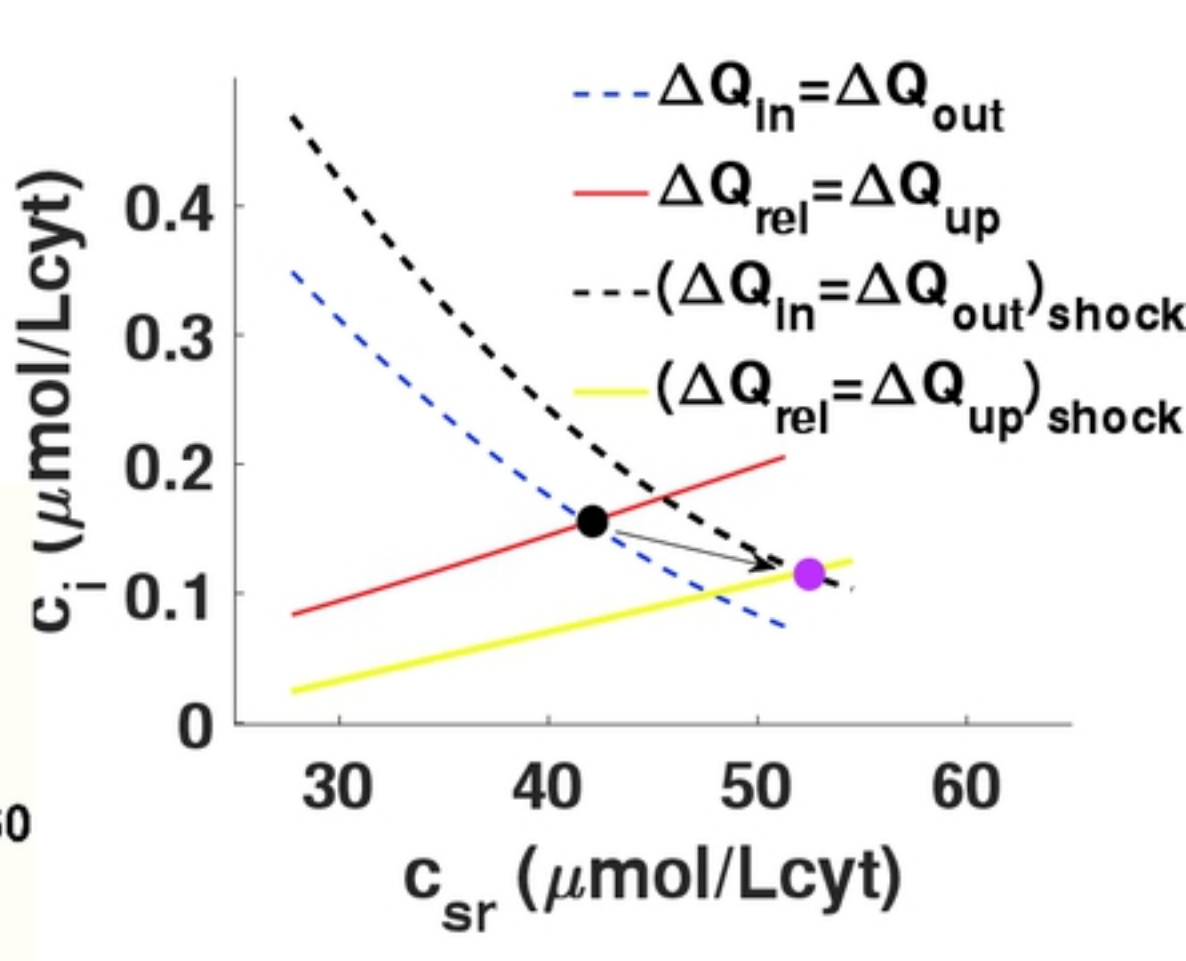

Figure 5

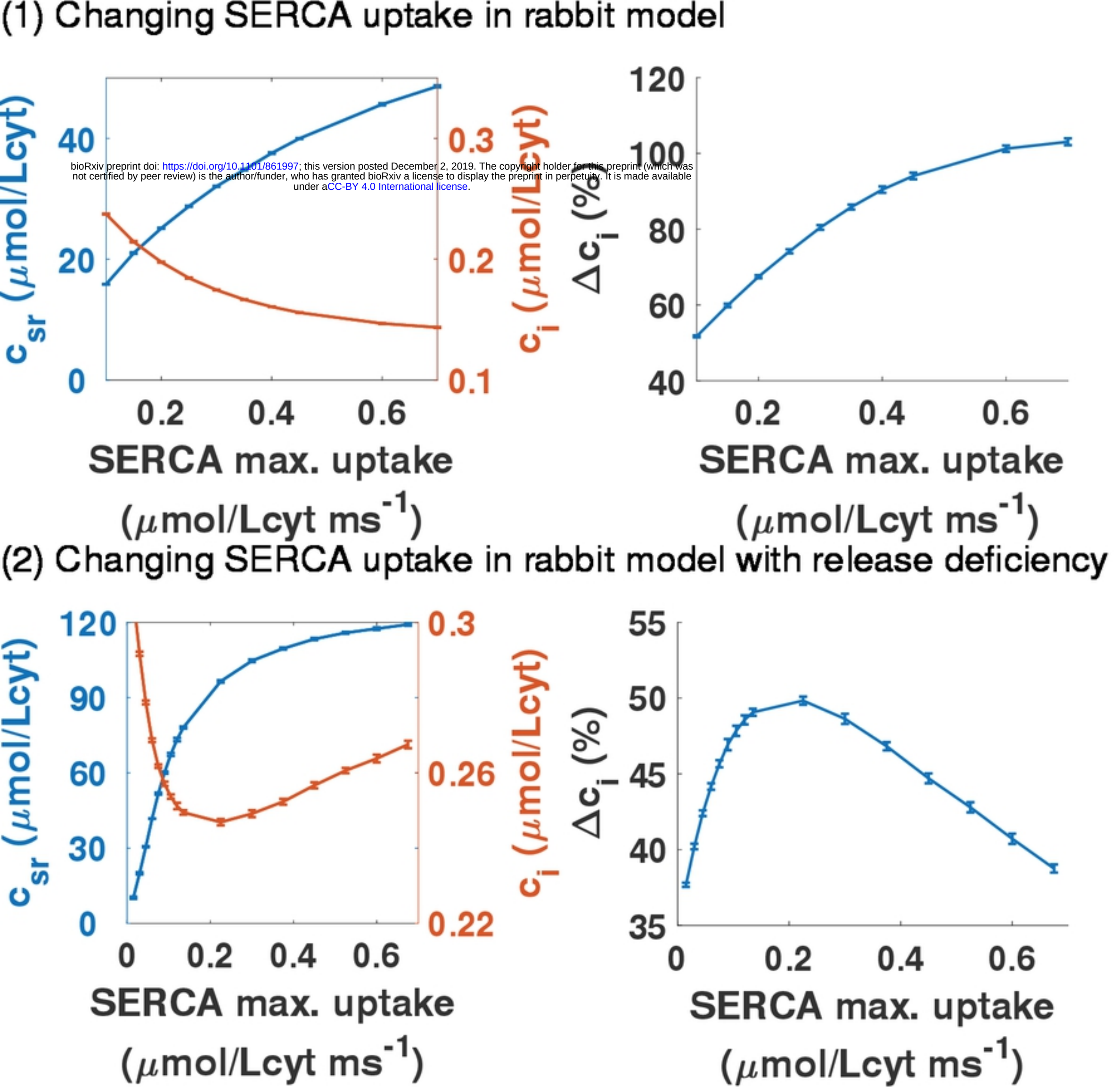

Figure 6

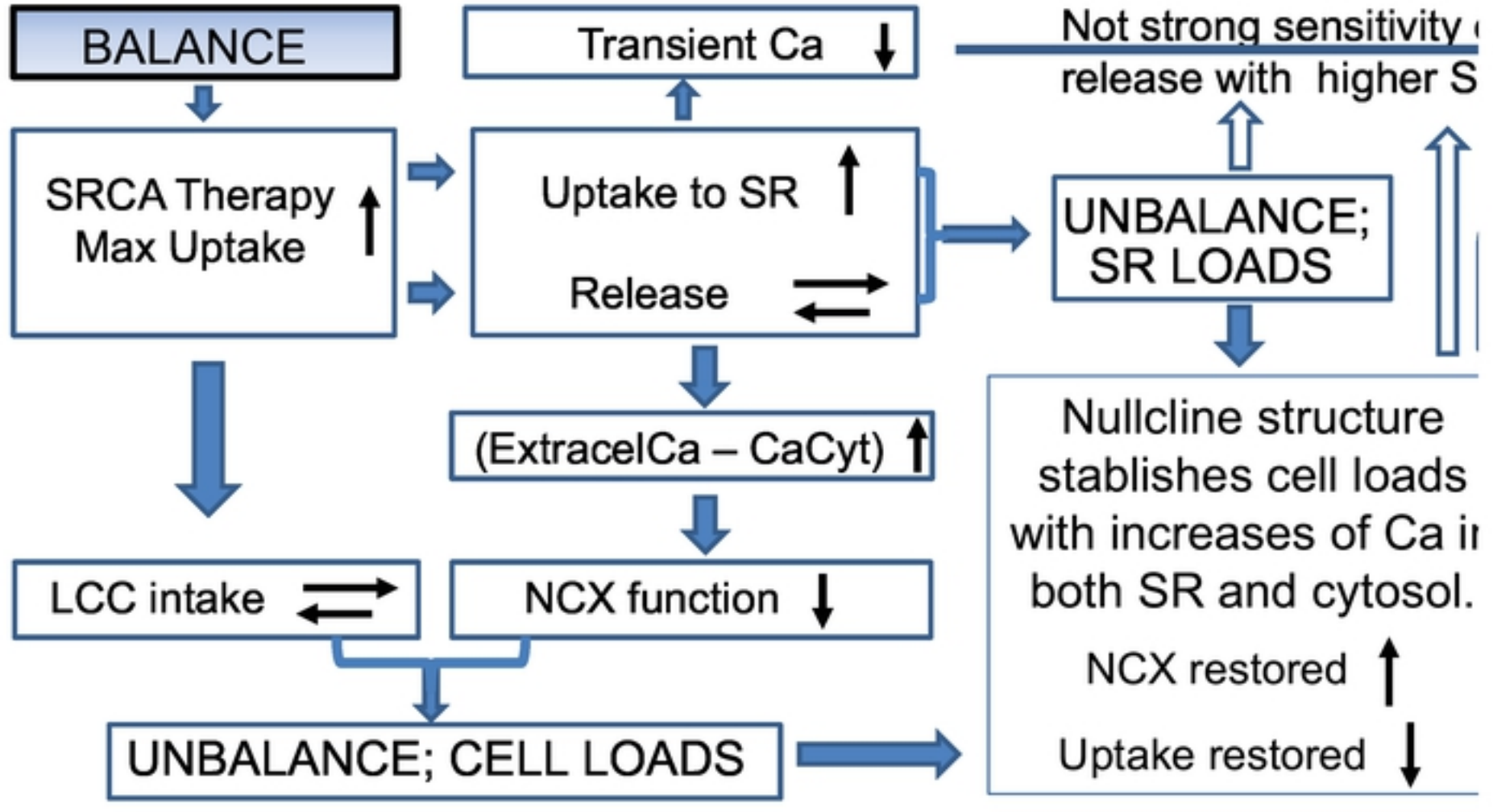
BALANCE
Transient Ca
Not strong sensitivity
release with higher S
SRCA Therapy
Max Uptake
Uptake to SR
Release
UNBALANCE;
SR LOADS
(ExtracelCa – CaCyt)
Nullcline structure
stablishes cell loads
with increases of Ca i
both SR and cytosol.
LCC intake
NCX function
NCX restored
UNBALANCE; CELL LOADS
Uptake restored

Figure 7